Arbitrarily structured laser pulses

Jacob R. Pierce, ^{1,*} John P. Palastro, ^{2,†} Fei Li, ¹ Bernardo Malaca, ³ Dillon Ramsey, ² Jorge Vieira, ³ Kathleen Weichman, ² and Warren B. Mori

¹Department of Physics and Astronomy, University of California, Los Angeles, California 90095, USA

² University of Rochester, Laboratory for Laser Energetics, Rochester, New York 14623, USA

³GoLP/Instituto de Plasmas e Fusão Nuclear, Instituto Superior Técnico, Universidade de Lisboa, Lisbon 1049-001, Portugal

(Received 28 July 2022; accepted 18 January 2023; published 7 February 2023)

Spatiotemporal control refers to a class of optical techniques for structuring a laser pulse with coupled spacetime-dependent properties, including moving focal points, dynamic spot sizes, and evolving orbital angular momenta. Here we introduce the concept of arbitrarily structured laser (ASTRL) pulses, which generalizes these techniques. The ASTRL formalism employs a superposition of prescribed pulses to create a desired electromagnetic field structure. Several examples illustrate the versatility of ASTRL pulses to address a broad range of laser-based applications, including laser wakefield acceleration, inertial confinement fusion, nanophotonics, and attosecond physics.

DOI: 10.1103/PhysRevResearch.5.013085

I. INTRODUCTION

Light can exhibit structures in space, time, or coupled spacetime. The realization that these structures can be shaped using optical techniques has led to a deeper understanding of the fundamental properties of light and advances in multiple laser-based applications. Spatial shaping involves the use of static optical elements, such as phase plates, deformable mirrors, or spatial light modulators, to form transverse structures with orbital angular momentum, Airy or Bessel profiles, or tailored speckle patterns [1–4]. Temporal shaping typically employs Fourier methods, in which frequency components are separated by diffraction gratings and separately modified, to synthesize pulses with nearly arbitrary time-dependent waveforms and polarizations [5,6].

Spatiotemporal pulse shaping invokes some combination of these techniques. Examples go back as far as smoothing by spectral dispersion (1989) [7] and pulse front tilt (1996) [8]. More modern examples include spatiotemporal optical vortices (STOVs) [9–11], diffraction-free light sheets [12–14], and flying focus concepts [15–18]. Flying focus pulses, in particular, feature intensity peaks with programmable trajectories that can travel distances far greater than a Rayleigh range while maintaining a near-constant profile. The trajectory control afforded by these pulses has been proposed as a means to overcome limitations of traditional pulses in a number of applications, including laser wakefield acceleration [19,20], Raman amplification [21], and nonlinear Thomson scattering [22], as well as for the exploration of fundamental physics,

Published by the American Physical Society under the terms of the Creative Commons Attribution 4.0 International license. Further distribution of this work must maintain attribution to the author(s) and the published article's title, journal citation, and DOI.

such as radiation reaction [23] and nonlinear Compton scattering [24].

Spatiotemporally structured pulses may be created using either a forward- or inverse-design approach. The forward-design approach requires identifying a specific solution to Maxwell's equations. Once known, this solution can be synthesized using programmable phase modulation techniques [25,26]. This is the approach taken to create light sheets, STOVs, and pulses with dynamic orbital angular momenta. However, this approach does not provide a method to systematically identify new solutions of Maxwell's equations with features that are desirable for a particular application. In the inverse-design approach, one imagines an electromagnetic structure with desirable features and synthesizes this structure using a superposition of solutions to Maxwell's equations with known properties. This is the approach presented here.

In this paper, we introduce a concept and theoretical formalism for generating laser pulses with arbitrary structure. These arbitrarily structured laser (ASTRL) pulses are synthesized using a superposition of traditional laser pulses with controlled and varying properties. The ASTRL formalism generalizes the creation of pulses with evolving focal points (flying foci), spot size, orbital angular momentum, and polarization, and can also describe pulses with exotic topological structure such as STOVs. An example of each of these is presented. The flexibility of the ASTRL concept opens new and previously unimagined possibilities for structured light with the potential to improve a wide range of laser-based applications, while its simplicity facilitates implementation into simulations.

II. THEORETICAL FORMALISM

The formulation of the ASTRL concept begins with the vacuum wave equation for the electric field of a laser pulse:

$$\left[\nabla^2 - \frac{1}{c^2}\partial_t^2\right] \mathbf{E}(\mathbf{x}, t) = 0.$$
 (1)

^{*}jacobpierce@physics.ucla.edu †jpal@lle.rochester.edu

ASTRL pulses are constructed by superposing solutions to Eq. (1) with varying properties. The electric field of an ASTRL pulse can be expressed either as a sum or an integral over these solutions:

$$\mathbf{E}(\mathbf{x},t) = \int d\eta \ \mathbf{E}_{\eta}(\mathbf{x},t), \tag{2}$$

where η parameterizes the varying properties of the solutions. For example, the amplitude, spot size, focal point, pulse duration, or relative delay of each \mathbf{E}_{η} can all depend on η . Equation (2) is the most general representation of an ASTRL pulse in vacuum.

Analytic solutions for \mathbf{E}_{η} simplify the process of designing an ASTRL pulse for a specific application. Paraxial solutions, in particular, are expressed in terms of familiar quantities that can be parameterized in terms of η . To derive such solutions, consider a laser pulse propagating in the \hat{z} direction with constant polarization $\hat{\epsilon}$. The transverse electric field can be expressed as an envelope $A(\mathbf{x}_{\perp}, z, t)$ modulated by a carrier

$$\mathbf{E}_{\perp}(\mathbf{x}_{\perp}, z, t) = \frac{1}{2}A(\mathbf{x}_{\perp}, z, t)e^{i(k_0z - \omega_0 t)}\hat{\boldsymbol{\epsilon}} + \text{c.c.}, \tag{3}$$

where k_0 is the central wavenumber and $\omega_0 = ck_0$. Substituting Eq. (3) into Eq. (1) and performing the Galilean change of variables $(\xi, s) = (z - ct, z)$ provides

$$\left[\nabla_{\perp}^{2} + \partial_{s}^{2} + 2ik_{0}\partial_{s} + 2\partial_{\xi}\partial_{s}\right]A(\mathbf{x}_{\perp}, s, \xi) = 0. \tag{4}$$

Upon applying the slowly varying envelope approximation $(|\partial_{\xi}|, |\partial_{s}| \ll k_{0})$, Eq. (4) reduces to

$$[\nabla_{\perp}^2 + 2ik_0\partial_s]A(\mathbf{x}_{\perp}, s, \xi) \approx 0.$$
 (5)

Equation (5) is the paraxial wave equation and its operator is independent of ξ . This independence admits separable solutions, i.e., solutions with no spatiotemporal coupling, of the form

$$A(\mathbf{x}_{\perp}, s, \xi) \approx B(\xi)C(\mathbf{x}_{\perp}, s),$$
 (6)

where $C(\mathbf{x}_{\perp}, s)$ satisfies $[\nabla_{\perp}^2 + 2ik_0\partial_s]C(\mathbf{x}_{\perp}, s) = 0$ and $B(\xi)$ is an arbitrary function. For example, $C(\mathbf{x}_{\perp}, s)$ may be any Laguerre-, Hermite-, or Ince-Gaussian mode and the longitudinal profile may be $B(\xi) = \exp[-(\xi/c\tau_0)^2]$.

The transverse electric field of a coherent ASTRL pulse can be approximated by summing or integrating over paraxial solutions:

$$\mathbf{E}_{\perp}(\mathbf{x}_{\perp}, s, \xi) \approx \frac{1}{2} e^{ik_0 \xi} \int d\eta \ B_{\eta}(\xi) C_{\eta}(\mathbf{x}_{\perp}, s) \hat{\boldsymbol{\epsilon}}(\eta) + \text{c.c.}, \quad (7)$$

where the properties of $B_{\eta}(\xi)$, $C_{\eta}(\mathbf{x}_{\perp}, s)$, and $\hat{\epsilon}(\eta)$ may vary with respect to η . The integral over η may introduce spatiotemporal coupling, such that in general, Eq. (7) cannot be written as a separable function. Thus, \mathbf{E}_{\perp} may possess a high degree of spatiotemporal coupling despite the absence of coupling in Eq. (6).

The η dependence of $B_{\eta}(\xi)$ may encode a delay $\Delta(\eta)$, duration $\tau_0(\eta)$, and weight $B_0(\eta)$ for each constituent pulse as

$$B_{\eta}(\xi) = B_0(\eta) \exp\left[-\left(\frac{\xi - \Delta(\eta)}{c\tau_0(\eta)}\right)^2\right]. \tag{8}$$

The durations $\tau_0(\eta)$ set the fastest timescale over which the properties of the ASTRL pulse can vary and determine

the number of pulses required for discrete approximation of Eq. (7). Unless otherwise stated, τ_0 and B_0 will be independent of η for the examples presented here.

A natural example for the η dependence of $C_{\eta}(\mathbf{x}_{\perp}, s)$ is an η -indexed Gaussian beam:

$$C_{\eta}(\mathbf{x}_{\perp}, s) = \left[\frac{z_{R}(\eta)}{q_{n}(s)}\right]^{d_{\perp}/2} \exp\left[-\frac{ik_{0}|\mathbf{x}_{\perp} - \mathbf{x}_{\perp 0}(\eta)|^{2}}{2q_{n}(s)}\right], \quad (9)$$

where $q_{\eta}(s) \equiv s - s_0(\eta) + iz_R(\eta)$ is the complex beam parameter and d_{\perp} is the number of transverse dimensions. In Eq. (9), the longitudinal focal position $s_0(\eta)$, transverse focal position $\mathbf{x}_{\perp 0}(\eta)$, and Rayleigh range $z_R(\eta)$ (and associated spot size $w_0(\eta) = \sqrt{2z_R(\eta)/k_0}$) may all be expressed as functions of the integration variable η , which allows for extended focal ranges and evolving transverse structure. More generally, the mode numbers of the transverse profile can depend on η , e.g., the radial or orbital angular momentum (OAM) quantum numbers of a Laguerre-Gaussian mode. Finally, $\hat{\epsilon}(\eta)$ may encode an evolving polarization.

III. DESIGN OF ASTRL PULSES

The utility and generality of the ASTRL concept will be demonstrated by using Eq. (7) to construct several examples of spatiotemporally structured laser pulses. To begin, consider the flying focus [15,16]. Each time slice in a flying focus pulse has a different focal point along the propagation axis. The time and location at which each slice comes to focus can be controlled to produce an intensity peak that travels at any velocity, including backwards or faster than the speed of light. Within the ASTRL formalism, a flying focus pulse may be described using a Gaussian transverse profile [Eq. (9)] with $\eta \in [-\frac{1}{2}, \frac{1}{2}]$ and $s_0(\eta) = \eta L$. This choice of $s_0(\eta)$ produces a focal range extending from s = -L/2 to s = L/2, where L can be much larger than z_R . At each s in the focal range, the focus will occur at a time determined by the condition $\xi = \Delta(\eta) = \Delta(s/L)$. The delay $\Delta(\eta)$ required for a given focal trajectory can be derived from geometric optics as in Ref. [19]. For example, motion of the focal point at a constant velocity $\mathbf{v}_f = c\beta_f$ is attained with $\Delta(\eta) = (1 - 1/\beta_f)L\eta$.

Figure 1(a) displays the on-axis envelope of a superluminal ($\beta_f = 1.05$) flying focus pulse obtained by evaluating Eq. (7). The white dashed line shows the space-time trajectory $z = v_f t$ and demonstrates that the laser envelope travels at the expected velocity over ten Rayleigh ranges. A finite-difference time-domain (FDTD) simulation of the full set of Maxwell's equations produces nearly identical results [Fig. 1(b)]. The simulation used Eq. (7) to initialize the fields, but did not make the approximations leading to Eq. (5). A slight discrepancy can be observed near $ct \approx 5z_R$ due to the inexactness of Eq. (6). The simulation was conducted using the code OSIRIS [27] with quasi-3D azimuthal decomposition [28] and the solver introduced in Ref. [29] to mitigate numerical dispersion.

The ASTRL concept can also be used to describe new types of generalized flying focus pulses. For instance, a pulse whose focal point oscillates in the transverse direction as it translates along the propagation axis could serve as a controllable wiggler for generating radiation from relativistic electron bunches or enhance direct laser acceleration of

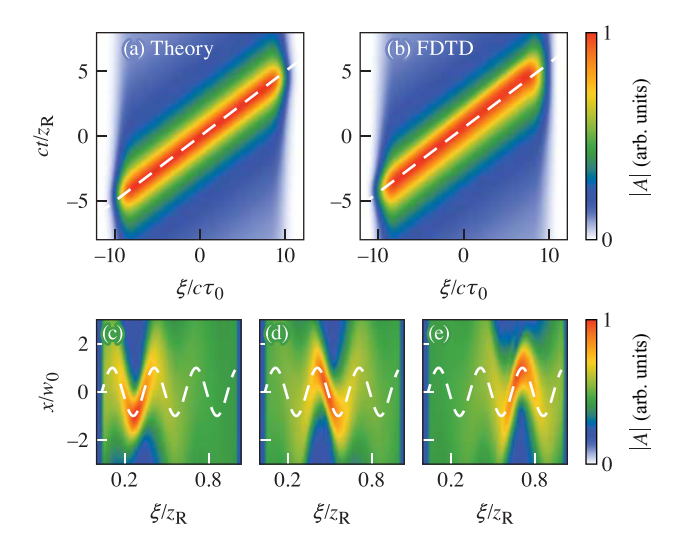


FIG. 1. (a) On-axis evolution of the envelope of an ASTRL flying focus pulse found by evaluating Eq. (7) with $k_0w_0=40$, $\omega_0\tau_0=20$, and $\beta_f=1.05$. The dashed line indicates the trajectory $z=v_ft$. (b) The envelope from a quasi-3D FDTD simulation for the same parameters. The two are in excellent agreement. (c)–(e) A generalized flying focus constructed using the ASTRL formalism in which the focal point oscillates transversely as it moves along the optical axis. The propagation was simulated in two dimensions using the FDTD method. The pulse was initialized at $ct/z_R=-10$ using Eq. (7) with $x_{\perp osc}=w_0$, $k_{osc}=1/z_R$, $\beta_f=1.05$, $L=20z_R$, $k_0w_0=40$, and $\omega_0\tau_0=20$. From left to right, the frames show the pulse at $ct/z_R=-4$, 0, and 4.

electrons through new parametric resonances. Such a pulse can be constructed by parametrizing both the transverse and longitudinal focal coordinates: $\mathbf{x}_{\perp 0}(\eta) = x_{\perp \rm osc} \sin[k_{\rm osc}s_0(\eta)]\mathbf{\hat{x}}$ and $s_0(\eta) = \eta L$, where, as before, $\eta \in [-\frac{1}{2},\frac{1}{2}]$. Figures 1(c)–1(e) display the envelope from two-dimensional OSIRIS simulations of this configuration. The intensity peak undergoes the expected oscillatory motion. Here, C_η is given by Eq. (9) and $\Delta(\eta) = (1-1/\beta_f)L\eta$, i.e., the focal point moves with a constant axial velocity.

Aside from moving focal points, many applications can benefit from pulses that have a fixed focal point with prescribed spatiotemporal profiles or time-dependent polarization (Fig. 2). Traditional Fourier techniques for temporal pulse shaping, as in Ref. [6], produce pulses described by Eq. (6) with a customized $B(\xi)$. Similarly, previous polarizationstructuring methods amount to evaluating Eq. (7) with a prescribed $\hat{\epsilon}(\eta)$ and B_{η} , but with a C_{η} that is independent of η . Figure 2(a) shows an example. This particular ASTRL pulse is constructed from a discrete sum of seven pulses, indexed by $\eta \in \{0, 1, \dots 6\}$, that share a common focal point, $s_0(\eta) = 0$. The delay and polarization of each pulse are given by $\Delta_{\eta} =$ $-2c\tau_0\eta$ and $\hat{\epsilon}(\eta) = [\cos(\pi\eta/5), \sin(\pi\eta/5), 0]$ while C_{η} is given by Eq. (9). Evolving polarization structures as in this example have led to advances in nonlinear spectroscopy [30], quantum control [31,32], nanophotonics [33], and a number of other areas [34,35]. More exotic pulses with continuous polarization evolution can also be described using the ASTRL concept.

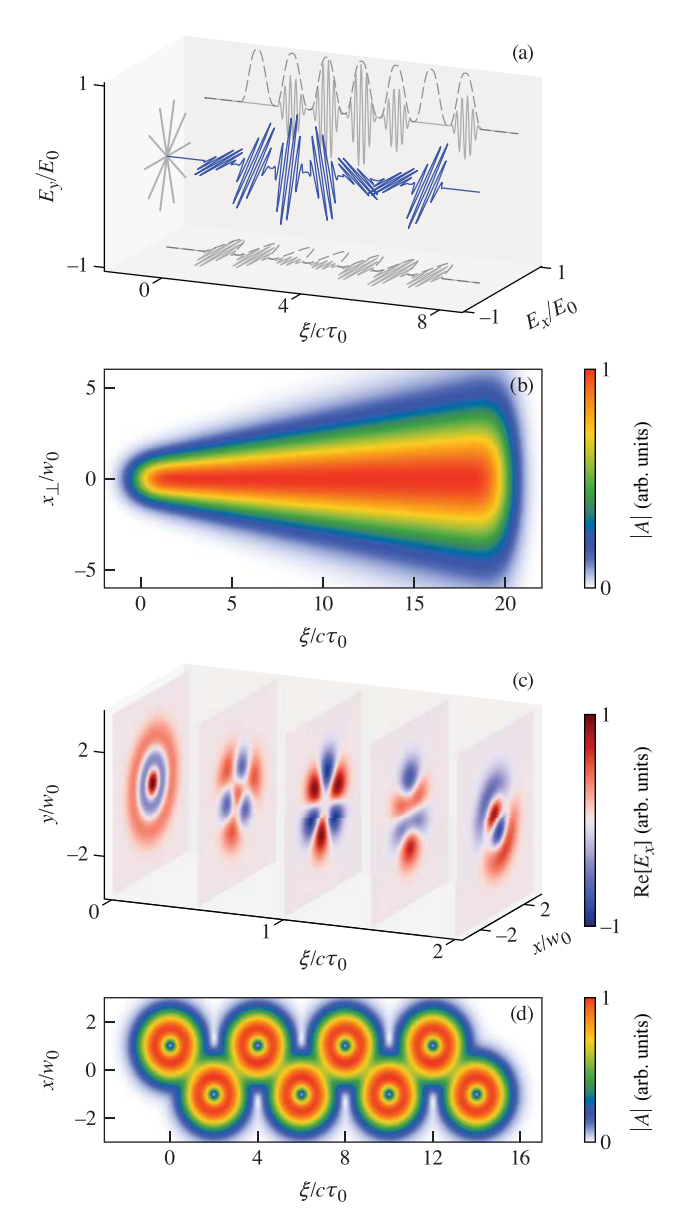


FIG. 2. Examples of ASTRL pulses constructed from superpositions of laser pulses focused to the same point $(s_0(\eta)=0)$: (a) A pulse everywhere linearly polarized, but with a time-dependent polarization angle. The duration of each pulse in the superposition is $\omega_0\tau_0=20$. (b) A laser pulse with a spot size that continuously decreases in time with $k_0w_{0\text{min}}=40$, $w_{0\text{max}}=4w_{0\text{min}}$, $\omega_0\tau_0=40$, and $\Delta_{\text{max}}=20c\tau_0$. (c) Time slices of the transverse electric field of a laser pulse whose angular momentum continuously evolves in time. (d) A lattice of STOVs with $k_0w_0=40$ and $\omega_0\tau_0=20$. All examples are evaluated using Eq. (7) and shown at the focal point s=0.

A time-dependent spot size can improve the performance of applications including laser wakefield acceleration [36] and inertial confinement fusion [37–39]. In laser wakefield acceleration, a spot size that increases in time can stabilize the propagation of an intense laser pulse in a plasma channel [36]. While in inertial confinement fusion, a spot size that decreases continuously in time can mitigate cross-beam energy transfer [37–39]. As demonstrated in Fig. 2(b), such a pulse can be described by Eqs. (7), (8), and (9) with a spot size

parameterized as $w_0(\eta) = w_{0\min} + \eta(w_{0\max} - w_{0\min})$ and the delay $\Delta(\eta) = -\Delta_{\max}\eta$, where $\eta \in [0, 1]$.

The orbital angular momentum and radial mode numbers (ℓ and p, respectively) of Laguerre-Gaussian modes provide additional degrees of freedom to structure the timedependence of the transverse profile. Figure 2(c) displays a sequence of time slices in an ASTRL pulse formed by superposing three pulses that partially overlap in time with $(\ell, p) =$ (0, 2), (3, 0), (1, 1). Each pulse is indexed by $\eta \in \{0, 1, 2\}$, has a delay $\Delta_{\eta} = -2c\tau_0\eta$, and a weight $B_0(\eta) = 1, 0.8, 1$. This construction produces a continuous transformation in angular momentum. In the first, third, and fifth frames, one pulse dominates, and the transverse profile is nearly a pure Laguerre-Gaussian mode; in the second and fourth frames, two pulses interfere to produce a hybrid mode. Investigations into structured OAM have only recently begun [25,26,40–42], but its potential for ultrafast probing of chiral systems has already drawn attention [42]. Many other applications based on OAM [43], including optical trapping and manipulation [44–47], imaging [48–50], quantum optics [51,52], nonlinear optics [53], and laser-plasma interactions [54-60], may also benefit from added control over its structure.

As a final example, the ASTRL concept can be used to construct STOVs. In fact, the vacuum STOV solution introduced in Ref. [9],

$$A(\mathbf{x}_{\perp}, s, \xi) = \left[\frac{\xi}{c\tau_0} \pm \frac{ix}{w(s)} \left(\frac{-q^*(s)}{q(s)} \right)^{1/2} \right] \frac{z_R}{q(s)}$$

$$\times \exp\left[-\frac{ik_0 x_{\perp}^2}{2q(s)} \right] \exp\left[-\left(\frac{\xi}{c\tau_0} \right)^2 \right], \quad (10)$$

is a superposition of two separable solutions as in Eq. (6), where the C_{η} functions are Hermite-Gaussian modes of order (0,0) and (1,0). Here the s dependence has been included, $w(s) \equiv w_0 \sqrt{1 + (s/z_R)^2}$, and $q^*(s)$ is the complex conjugate of q(s). The generalization of Eq. (10) to higher-order vortex topologies (see Ref. [11]) can also be expressed as a superposition of separable solutions. Figure 2(d) illustrates a novel STOV lattice assembled by superposing solutions in the form of Eq. (10). The solutions are indexed by $\eta \in \{0, 1, ..., 7\}$ with delays $\Delta_{\eta} = -2c\tau_0\eta$, transverse displacements alternating between $x_0 = \pm w_0$, and polarities [the sign in Eq. (10)] alternating between ± 1 .

IV. EXPERIMENTAL APPROACHES TO SYNTHESIZING ASTRL PULSES

Optical configurations for producing specific subclasses of ASTRL pulses have already been proposed or experimentally realized [10,15,16,19]. These configurations may be modified to produce new kinds of ASTRL pulses informed by Eq. (7), such as the oscillating flying focus in Figs. 1(c)–1(e). In addition, experimental approaches for synthesis of arbitrary solutions of Maxwell's equations as in Refs. [25,26] can be used to create solutions designed using the ASTRL approach. Here we propose a different approach, based on recent developments in divided pulse amplification, which enables synthesis of more general classes of ASTRL pulses.

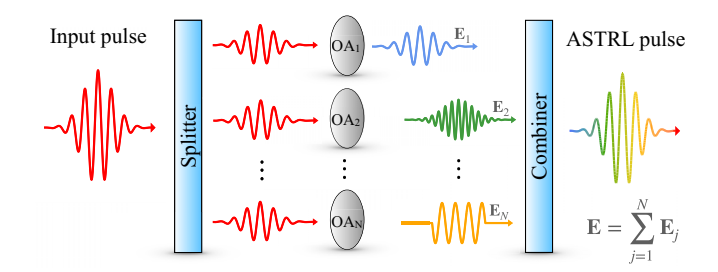


FIG. 3. An experimental concept to produce new classes of ASTRL pulses. Each pulse is independently manipulated by a separate optical assembly, labeled " OA_j ", which can alter the amplitude, transverse profile, frequency, delay, or other properties. The pulses are then coherently combined to form an ASTRL pulse.

Wavelength-multiplexed communication and power scaling have motivated decades of progress in methods for combining continuous-wave laser beams [61–64]. Conceptually, N independent beams or N copies of one beam are individually amplified and then recombined into a single beam with N times the original power. Splitting and recombination are achieved using standard optics, such as diffraction gratings, fibers, and beam splitters. More recently, these methods have been applied to ultrashort laser pulses as a path towards pulses beyond the petawatt class [65–73], with coherent combinations of up to 81 pulses [74].

Divided pulse amplification techniques can be extended to produce ASTRL pulses. In addition to being amplified, the separated pulses can be independently focused, delayed, polarization-rotated, or altered in other ways before being recombined. Figure 3 shows a schematic of the proposed experimental concept in which different optical assemblies independently manipulate each of the divided pulses. As an example, optical assemblies composed of a spiral phase plate and delay stage could produce a pulse with continuously evolving OAM as in Fig. 2(c); alternatively, using a half-waveplate and delay stage could produce a pulse with continuously evolving polarization as in Fig. 2(a). Despite the potential challenges of alignment and timing, divided pulse manipulation could provide unprecedented control over the structure of the combined pulse and enable creation of the broad class of pulses described by Eq. (7). Note that Ref. [42] has used a special case of this concept to combine two pulses with different OAM; the combined pulse was used to drive high-harmonic attosecond pulses.

This approach to synthesizing ASTRL pulses is based on approximating the integral in Eq. (7) as a discrete sum of pulses. To illustrate this, consider the $\beta_f = 1.05$ flying focus example shown in Fig. 1. Figure 4 demonstrates that 20 pulses are more than sufficient to approximate the integral when $L = 10z_R$.

More generally, the minimum number of laser pulses required to approximate Eq. (7) can be estimated by ensuring that the sum-total duration of all constituent pulses is greater than the duration of the entire ASTRL pulse T, i.e., $N \gtrsim T/\tau_0$. For a flying focus pulse, the effective duration of the intensity peak, $\tau_{\rm eff} = (1 - \beta_f)z_R/v_f$ [18], satisfies $\tau_{\rm eff}/T = z_R/L$, which implies that $N \gtrsim (1 - \beta_f)L/v_f\tau_0$ pulses are required. Note, however, that for certain applications, discrete

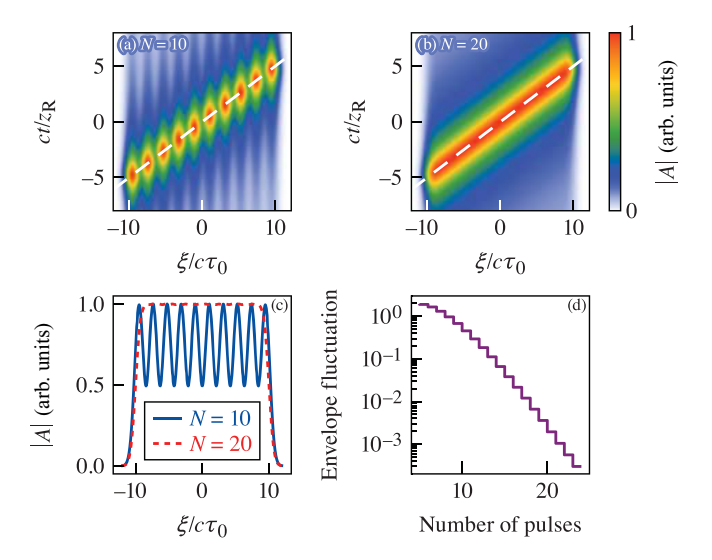


FIG. 4. (a), (b) Discrete approximations of Eq. (7) for the β_f = 1.05 flying focus pulse shown in Fig. 1 with N=10 and N=20 pulses, respectively; the continuum is well approximated by 20 pulses, or 2 pulses per z_R . (c) Peak on-axis amplitude for the N=10 and 20 cases, showing oscillation for N=10. (d) Relative amplitude oscillation, defined as $(\max |A| - \min |A|)/(\max |A| + \min |A|)$ over the interval $[-z_R, z_R]$. The relative oscillation decreases exponentially with N, which determines the number of pulses required for a given tolerance.

separation of the constituent pulses as in the N=10 case of Fig. 4 may also be desirable.

V. ACCURACY OF EQ. (6)

As demonstrated by the examples above, an ASTRL pulse may generally exhibit spatiotemporal coupling despite being assembled from pulses with no spatiotemporal coupling [i.e., Eq. (6)]. The separability of Eq. (6) was derived by reducing the full wave equation [Eq. (4)] to the paraxial wave equation [Eq. (5)]. The validity of the approximations leading to Eq. (5) may be determined by evaluating derivatives of the approximate solution $A(\mathbf{x}_{\perp}, s, \xi) = z_R/q(s) \exp[-ik_0x_{\perp}^2/2q(s)] \exp[-(\xi/c\tau_0)^2]$. At any location, $|\partial_s^2 A| \ll |2ik_0\partial_s A|$ when $k_0w_0 \gg 1$; this is the usual paraxial approximation, which fails only for tightly focused laser pulses. On the other hand, $|2\partial_{\xi}\partial_s A| \ll |2ik_0\partial_s A|$ when $\omega_0\tau_0 \gg 1$. This condition only fails for pulses with durations less than a few cycles. These two conditions, i.e., $k_0w_0 \gg 1$ and $\omega_0\tau_0 \gg 1$, place constraints on C_{η} and B_{η} , respectively.

For an envelope that is initially separable at some $s=s_i$, spatiotemporal coupling will develop beyond a range $|s-s_i|\gtrsim L_{\rm stc}\equiv \frac{1}{2}c\tau_0k_0^2w_0^2$ because of the $\partial_\xi\partial_z$ term in Eq. (4) (see Appendix A). There are two common scenarios that can be considered. In the first scenario, every pulse comprising an ASTRL pulse is separable at its focus. Because each pulse only contributes significantly within a Rayleigh range of its focus, the condition on the accuracy of Eq. (6) can be expressed as $L_{\rm stc}\gtrsim z_R$ or, equivalently, $\omega_0\tau_0\gtrsim 1$. In the second scenario, which is more applicable to field initialization in a simulation, every pulse is separable at a specified

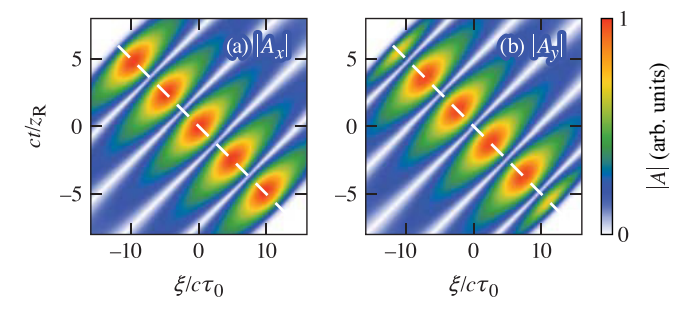


FIG. 5. (a), (b) On-axis evolution of the vector envelope for a negative-velocity flying focus with structured polarization. The vector envelope is defined as $A_j \equiv \hat{\mathbf{e}}_j \cdot \int d\eta \ B_{\eta}(\xi) C_{\eta}(\mathbf{x}_{\perp}, s) \hat{\mathbf{e}}(\eta)$. The parameters are identical to those in Fig. 1 except $\beta_f = -1$ and the polarization evolves continuously. Specifically, $\hat{\mathbf{e}}_x(\eta) = \cos(k_{\rm osc}\eta L)$ and $\hat{\mathbf{e}}_y(\eta) = \sin(k_{\rm osc}\eta L)$, where $k_{\rm osc} = (3/2)z_R^{-1}$. The white dashed lines indicate the focal trajectory z = -ct. Both plots are evaluated using Eq. (7).

distance L_{η} from focus. The condition on the accuracy of Eq. (6) is then given by $L_{\rm stc} \gtrsim \max_{\eta} L_{\eta}$. For example, in Figs. 1(a)–1(b) $\max_{\eta} L_{\eta} = \frac{1}{2} L_{\rm stc}$, which contributes to the slight discrepancy at the end of the focal region. However, even if $L_{\rm stc} \lesssim \max_{\eta} L_{\eta}$ and spatiotemporal coupling develops in the constituent pulses, the qualitative features of the desired electromagnetic structure would remain intact.

VI. DISCUSSION AND CONCLUSION

In addition to facilitating the creation of new and previously unimagined electromagnetic structures, the ASTRL formalism simplifies the injection of structured light in simulations. Previous simulations of flying focus pulses required a Fresnel integral to propagate the field from the optic plane of a specific experimental design to the simulation plane. In contrast, the ASTRL description enables direct field initialization in the simulation plane, which simplifies implementation. Further, by decoupling the structured light-matter interaction physics from the details of a particular optical configuration, the ASTRL description expedites prototyping of new concepts. For example, the axiparabola-echelon pair used in Ref. [19] would not need to be redesigned for every simulation. An optical configuration capable of delivering the desired pulse can be designed or implemented in a simulation after a concept shows promise.

The generality of the ASTRL concept extends well beyond Eq. (7) and the examples presented here. The time dependence of any combination of parameters can be simultaneously structured. For instance, a negative-velocity flying focus can be combined with continuously evolving polarization (Fig. 5). Further, the ASTRL concept can be extended to accommodate multicolor pulses [75,76], superpositions of pulses with vector polarization [77–80], and pulses structured in the spatiospectral domain. In fact, using a wavelet transform one can show that arbitrary monochromatic laser fields may be decomposed as a generalized version of Eq. (7) (see Appendix B).

The ASTRL formalism provides a framework for constructing laser pulses with desired spatiotemporal structure. An ASTRL pulse is synthesized using superpositions of

known solutions to Maxwell's equations, such as an ensemble of traditional laser pulses. The flexibility of the ASTRL concept was illustrated with several examples, including pulses with moving focal points, dynamic polarization, evolving angular momentum, and nontrivial topological structure. In practice, ASTRL pulses can be synthesized using a number of experimental techniques, including the divided pulse manipulation scheme proposed here. New pulses based on the ASTRL concept may enable or enhance techniques in a range of scientific disciplines, including microscopy, nonlinear optics, quantum optics, and laser-plasma interactions.

ACKNOWLEDGMENTS

The authors graciously acknowledge C. Joshi, D. H. Froula, M. Vranic, E. P. Alves, SJ Spencer, A. Di Piazza, M. Formanek, T. Carbin, and C. Barkan for their lucid insights. Work supported by the National Science Foundation Award No. 2108970, the Department of Energy Contracts No. DE-SC00215057 and No. DE-SC0010064, the Scientific Discovery through Advanced Computing (SciDAC) program through a Fermi National Accelerator Laboratory (FNAL) subcontract No. 644405, and the University of Rochester, Laboratory for Laser Energetics. Computer simulations were performed on NERSC's Cori cluster (account m1157). J.R.P. was partially supported by a scholarship from the Directed Energy Professional Society.

APPENDIX A: LENGTH SCALE FOR EMERGENCE OF SPATIOTEMPORAL COUPLING

Over a long enough propagation path, the $2\partial_s \partial_{\xi}$ term omitted in Eq. (5) will lead to the development of spatiotemporal coupling in an initially separable envelope. The length scale over which this coupling develops can be estimated using geometric optics. Consider a pulse initialized by Eq. (6) at $s = -s_0$ with a focal point at s = 0. The distance from a radial location r to the focal point is given by $d(r) = \sqrt{r^2 + s_0^2}$. The separable form of Eq. (6) begins to break down when the delay between the center and outer radii of the pulse becomes comparable to its duration τ_0 . For an initial Gaussian transverse profile, the spot size at $s = -s_0$ is $w(-s_0) \approx w_0 s_0/z_R = 2s_0/k_0 w_0$, where w_0 is the spot size at focus. Setting r = w provides the delay $\Delta \sim \sqrt{(2s_0/k_0w_0)^2 + s_0^2} - s_0 \sim 2s_0/(k_0w_0)^2$. Equating $\Delta \gtrsim$ $c\tau_0$ demonstrates that Eq. (6) breaks down for propagation distances

$$s_0 \gtrsim L_{\text{stc}} \equiv \frac{1}{2}c\tau_0 k_0^2 w_0^2. \tag{A1}$$

For most pulses of interest, $\omega_0 \tau_0 \gg 1$ so that $L_{\rm stc} \gg z_R$, i.e., Eq. (6) remains valid over distances much longer than a Rayleigh range.

Equation (A1) can also be derived using a multiscale expansion of the operators in Eq. (4), where it is explicitly assumed that the mixed derivative term is a first-order correction. The ∂_s operator on the full solution A may be expanded as $\partial_s \approx \partial_{s0} + \partial_{s1}$, where $\partial_{s0} \gg \partial_{s1}$. To lowest order, $k_0 \partial_{s0}$ balances ∇_{\perp}^2 and one finds the scaling, $\partial_{s0} \sim z_R^{-1}$. At first order, $k_0 \partial_{s1}$ balances $\partial_{s0} \partial_{\xi}$, providing the scaling relation $k_0/L_{\text{stc}} \approx 1/c\tau_0 z_R$. Upon solving for L_{stc} , this simplifies to Eq. (A1).

APPENDIX B: SEPARABLE ENVELOPE DECOMPOSITION OF ARBITRARY LASER FIELDS

Consider an electric field with characteristics of a monochromatic laser pulse, i.e., a power spectrum peaked at a single ω_0 such that $\omega_0\tau_0\gtrsim 1$, but otherwise arbitrary structure. It is possible to show that such an arbitrary field may be decomposed as a superposition of separable pulses through a generalization of Eq. (7). In particular, the envelope may be exactly decomposed as

$$A(\mathbf{x}_{\perp}, s, \xi) = C_{\psi}^{-1} \int_{\mathbb{R}} \int_{\mathbb{R}} \frac{da \, db}{a^2 |a|^{1/2}} C^{(a,b)}(\mathbf{x}_{\perp}, s) \psi\left(\frac{\xi - b}{a}\right)$$
(B1)

where C_{ψ}^{-1} is a constant, ψ is a wavelet mother function, and

$$C^{(a,b)}(\mathbf{x}_{\perp},s) = \frac{1}{|a|^{1/2}} \int_{\mathbb{R}} d\xi \, A(\mathbf{x}_{\perp},s,\xi) \psi^* \left(\frac{\xi-b}{a}\right) \quad (B2)$$

is the wavelet transform of $A(\mathbf{x}_{\perp}, s, \xi)$ with respect to ξ for fixed \mathbf{x}_{\perp} and s [81]. For example, one may use the Ricker wavelet $\psi(g) = \psi_0 \exp[-g^2/2](1-g^2)$. In Eq. (B1), a and b are, respectively, the length and delay of each constituent pulse. The properties of each $C^{(a,b)}(\mathbf{x}_{\perp}, s)$, such as spot size and focal point, may depend on a and b.

Equation (B1) is a superposition of separable pulses at each slice in s. Given initial data for the envelope $A(\mathbf{x}_{\perp}, 0, \xi)$ at some slice s = 0, the decomposition may be used to approximately evolve the full solution $A(\mathbf{x}_{\perp}, s, \xi)$ using Eq. (6) as

$$A(\mathbf{x}_{\perp}, s, \xi) \approx C_{\psi}^{-1} \int_{\mathbb{R}} \int_{\mathbb{R}} \frac{da \, db}{a^2 |a|^{1/2}} C_{\text{parax}}^{(a,b)}(\mathbf{x}_{\perp}, s) \psi\left(\frac{\xi - b}{a}\right), \tag{B3}$$

where $C_{\text{parax}}^{(a,b)}(\mathbf{x}_{\perp},s)$ are solutions to the paraxial wave equation $[2ik_0\partial_s + \nabla_{\perp}^2]C_{\text{parax}}(\mathbf{x}_{\perp},s) = 0$ with initial condition $C_{\text{parax}}(\mathbf{x}_{\perp},0) = C^{(a,b)}(\mathbf{x}_{\perp},0)$. The properties of $C_{\text{parax}}^{(a,b)}$ determine the range of s over which Eq. (B3) remains valid. For example, if $C_0^{(a,b)}(\mathbf{x}_{\perp})$ resembles a Gaussian beam with spot size $w_0(a,b)$ for each (a,b), then Eq. (B3) remains valid when

$$|s| \lesssim \min_{a,b} L_{\text{stc}}(a,b) = \min_{a,b} ak_0^2 w_0(a,b)^2,$$
 (B4)

where the minimum is taken over (a, b) with significant contribution to the integral in Eq. (B1). Note that the specific choice of wavelet is not important, but the wavelet determines the conditions required for validity of Eq. (B3).

Equation (B3) generalizes Eq. (7) and shows that any fully coherent laser pulse solution may be approximately decomposed as a superposition of pulses with separable envelopes. In this sense, all monochromatic laser pulses can be constructed as ASTRL pulses. However, we restrict the scope of ASTRL pulses to include pulses that have been intentionally designed to exhibit a particular structure either through Eq. (2) or Eq. (7).

- [1] M. Beijersbergen, R. Coerwinkel, M. Kristensen, and J. Woerdman, Helical-wavefront laser beams produced with a spiral phaseplate, Opt. Commun. 112, 321 (1994).
- [2] G. A. Siviloglou, J. Broky, A. Dogariu, and D. N. Christodoulides, Observation of Accelerating Airy Beams, Phys. Rev. Lett. 99, 213901 (2007).
- [3] N. Chattrapiban, E. A. Rogers, D. Cofield, I. Wendell T. Hill, and R. Roy, Generation of nondiffracting bessel beams by use of a spatial light modulator, Opt. Lett. 28, 2183 (2003).
- [4] Y. Kato, K. Mima, N. Miyanaga, S. Arinaga, Y. Kitagawa, M. Nakatsuka, and C. Yamanaka, Random Phasing of High-Power Lasers for Uniform Target Acceleration and Plasma-Instability Suppression, Phys. Rev. Lett. 53, 1057 (1984).
- [5] T. Brixner and G. Gerber, Femtosecond polarization pulse shaping, Opt. Lett. 26, 557 (2001).
- [6] A. M. Weiner, Ultrafast optical pulse shaping: A tutorial review, Opt. Commun. 284, 3669 (2011).
- [7] S. Skupsky, R. Short, T. Kessler, R. Craxton, S. Letzring, and J. Soures, Improved laser-beam uniformity using the angular dispersion of frequency-modulated light, J. Appl. Phys. 66, 3456 (1989).
- [8] J. Hebling, Derivation of the pulse front tilt caused by angular dispersion, Opt. Quantum Electron. 28, 1759 (1996).
- [9] N. Jhajj, I. Larkin, E. W. Rosenthal, S. Zahedpour, J. K. Wahlstrand, and H. M. Milchberg, Spatiotemporal Optical Vortices, Phys. Rev. X 6, 031037 (2016).
- [10] S. Hancock, S. Zahedpour, A. Goffin, and H. Milchberg, Free-space propagation of spatiotemporal optical vortices, Optica 6, 1547 (2019).
- [11] S. W. Hancock, S. Zahedpour, and H. M. Milchberg, Mode Structure and Orbital Angular Momentum of Spatiotemporal Optical Vortex Pulses, Phys. Rev. Lett. 127, 193901 (2021).
- [12] H. E. Kondakci and A. F. Abouraddy, Diffraction-free pulsed optical beams via space-time correlations, Opt. Express 24, 28659 (2016).
- [13] H. E. Kondakci and A. F. Abouraddy, Diffraction-free spacetime light sheets, Nat. Photon. 11, 733 (2017).
- [14] H. Kondakci and A. F. Abouraddy, Optical space-time wave packets having arbitrary group velocities in free space, Nature Commun. 10, 929 (2019).
- [15] A. Sainte-Marie, O. Gobert, and F. Quéré, Controlling the velocity of ultrashort light pulses in vacuum through spatiotemporal couplings, Optica 4, 1298 (2017).
- [16] D. H. Froula, D. Turnbull, A. S. Davies, T. J. Kessler, D. Haberberger, J. P. Palastro, S.-W. Bahk, I. A. Begishev, R. Boni, S. Bucht, J. Katz, and J. L. Shaw, Spatiotemporal control of laser intensity, Nat. Photon. 12, 262 (2018).
- [17] T. T. Simpson, D. Ramsey, P. Franke, N. Vafaei-Najafabadi, D. Turnbull, D. H. Froula, and J. P. Palastro, Nonlinear spatiotemporal control of laser intensity, Opt. Express 28, 38516 (2020).
- [18] T. T. Simpson, D. Ramsey, P. Franke, K. Weichman, M. V. Ambat, D. Turnbull, D. H. Froula, and J. P. Palastro, Spatiotemporal control of laser intensity through cross-phase modulation, Opt. Express 30, 9878 (2022).
- [19] J. P. Palastro, J. L. Shaw, P. Franke, D. Ramsey, T. T. Simpson, and D. H. Froula, Dephasingless Laser Wakefield Acceleration, Phys. Rev. Lett. 124, 134802 (2020).
- [20] C. Caizergues, S. Smartsev, V. Malka, and C. Thaury, Phase-locked laser-wakefield electron acceleration, Nat. Photon. 14, 475 (2020).

- [21] D. Turnbull, S. Bucht, A. Davies, D. Haberberger, T. Kessler, J. L. Shaw, and D. H. Froula, Raman Amplification with a Flying Focus, Phys. Rev. Lett. 120, 024801 (2018).
- [22] D. Ramsey, B. Malaca, A. Di Piazza, M. Formanek, P. Franke, D. H. Froula, M. Pardal, T. T. Simpson, J. Vieira, K. Weichman, and J. P. Palastro, Nonlinear thomson scattering with ponderomotive control, Phys. Rev. E 105, 065201 (2022).
- [23] M. Formanek, D. Ramsey, J. P. Palastro, and A. Di Piazza, Radiation reaction enhancement in flying focus pulses, Phys. Rev. A 105, L020203 (2022).
- [24] A. Di Piazza, Unveiling the transverse formation length of nonlinear compton scattering, Phys. Rev. A 103, 012215 (2021).
- [25] D. Cruz-Delgado, S. Yerolatsitis, N. K. Fontaine, D. N. Christodoulides, R. Amezcua-Correa, and M. A. Bandres, Synthesis of ultrafast wavepackets with tailored spatiotemporal properties, Nat. Photon. 16, 686 (2022).
- [26] L. Chen, W. Zhu, P. Huo, J. Song, H. J. Lezec, T. Xu, and A. Agrawal, Synthesizing ultrafast optical pulses with arbitrary spatiotemporal control, Sci. Adv. 8, eabq8314 (2022).
- [27] R. A. Fonseca, L. O. Silva, F. S. Tsung, V. K. Decyk, W. Lu, C. Ren, W. B. Mori, S. Deng, S. Lee, T. Katsouleas, and J. C. Adam, OSIRIS: A three-dimensional, fully relativistic particle in cell code for modeling plasma based accelerators, in *Computational Science ICCS 2002*, edited by P. M. A. Sloot, C. J. Kenneth Tan, J. J. Dongarra, and A. G. Hoekstra, Lecture Notes in Computer Science Vol. 2331 (Springer, Berlin, 2002), pp. 342–351.
- [28] A. Davidson, A. Tableman, W. An, F. Tsung, W. Lu, J. Vieira, R. Fonseca, L. Silva, and W. Mori, Implementation of a hybrid particle code with a PIC description in *r*–*z* and a gridless description in *φ* into OSIRIS, J. Comput. Phys. **281**, 1063 (2015).
- [29] F. Li, K. G. Miller, X. Xu, F. S. Tsung, V. K. Decyk, W. An, R. A. Fonseca, and W. B. Mori, A new field solver for modeling of relativistic particle-laser interactions using the particle-incell algorithm, Comput. Phys. Commun. 258, 107580 (2021).
- [30] Y. Silberberg, Quantum coherent control for nonlinear spectroscopy and microscopy, Annu. Rev. Phys. Chem. 60, 277 (2009).
- [31] D. M. Villeneuve, S. A. Aseyev, P. Dietrich, M. Spanner, M. Y. Ivanov, and P. B. Corkum, Forced Molecular Rotation in an Optical Centrifuge, Phys. Rev. Lett. 85, 542 (2000).
- [32] T. Brixner, G. Krampert, T. Pfeifer, R. Selle, G. Gerber, M. Wollenhaupt, O. Graefe, C. Horn, D. Liese, and T. Baumert, Quantum Control by Ultrafast Polarization Shaping, Phys. Rev. Lett. 92, 208301 (2004).
- [33] M. Aeschlimann, M. Bauer, D. Bayer, T. Brixner, F. J. García de Abajo, W. Pfeiffer, M. Rohmer, C. Spindler, and F. Steeb, Adaptive subwavelength control of nano-optical fields, Nature (London) 446, 301 (2007).
- [34] H. Rubinsztein-Dunlop, A. Forbes, M. V. Berry, M. R. Dennis, D. L. Andrews, M. Mansuripur, C. Denz, C. Alpmann, P. Banzer, T. Bauer *et al.*, Roadmap on structured light, J. Opt. 19, 013001 (2017).
- [35] K. Misawa, Applications of polarization-shaped femtosecond laser pulses, Adv. Phys.: X 1, 544 (2016).
- [36] C. Benedetti, C. B. Schroeder, E. Esarey, and W. P. Leemans, Quasi-matched propagation of high-intensity, ultra-short laser pulses in plasma channels, AIP Conf. Proc. 1507, 252 (2012).
- [37] I. V. Igumenshchev, D. H. Froula, D. H. Edgell, V. N. Goncharov, T. J. Kessler, F. J. Marshall, R. L. McCrory, P. W.

- McKenty, D. D. Meyerhofer, D. T. Michel, T. C. Sangster, W. Seka, and S. Skupsky, Laser-Beam Zooming to Mitigate Crossed-Beam Energy Losses in Direct-Drive Implosions, Phys. Rev. Lett. **110**, 145001 (2013).
- [38] D. Froula, T. Kessler, I. Igumenshchev, R. Betti, V. Goncharov, H. Huang, S. Hu, E. Hill, J. Kelly, D. Meyerhofer *et al.*, Mitigation of cross-beam energy transfer: Implication of two-state focal zooming on omega, Phys. Plasmas 20, 082704 (2013).
- [39] X. Huang, D. Hu, W. Zhou, W. Dai, X. Deng, Q. Yuan, Q. Zhu, and F. Jing, Optical zooming based on focusing grating in direct drive ICF, Opt. Express **24**, 22051 (2016).
- [40] Z. Zhou, C. Min, H. Ma, Y. Zhang, X. Xie, H. Zhan, and X. Yuan, Time-varying orbital angular momentum in tight focusing of ultrafast pulses, Opt. Express 30, 13416 (2022).
- [41] L. Rego, K. M. Dorney, N. J. Brooks, Q. L. Nguyen, C.-T. Liao, J. San Román, D. E. Couch, A. Liu, E. Pisanty, M. Lewenstein *et al.*, Generation of extreme-ultraviolet beams with time-varying orbital angular momentum, Science 364, eaaw9486 (2019).
- [42] K. M. Dorney, L. Rego, N. J. Brooks, J. San Román, C.-T. Liao, J. L. Ellis, D. Zusin, C. Gentry, Q. L. Nguyen, J. M. Shaw et al., Controlling the polarization and vortex charge of attosecond high-harmonic beams via simultaneous spin—orbit momentum conservation, Nat. Photon. 13, 123 (2019).
- [43] L. Allen, M. W. Beijersbergen, R. J. C. Spreeuw, and J. P. Woerdman, Orbital angular momentum of light and the transformation of laguerre-gaussian laser modes, Phys. Rev. A 45, 8185 (1992).
- [44] H. He, N. Heckenberg, and H. Rubinsztein-Dunlop, Optical particle trapping with higher-order doughnut beams produced using high efficiency computer generated holograms, J. Mod. Opt. 42, 217 (1995).
- [45] K. Gahagan and G. J. Swartzlander, Optical vortex trapping of particles, Opt. Lett. **21**, 827 (1996).
- [46] P. Prentice, M. MacDonald, T. Frank, A. Cuschieri, G. Spalding, W. Sibbett, P. Campbell, and K. Dholakia, Manipulation and filtration of low index particles with holographic laguerregaussian optical trap arrays, Opt. Express 12, 593 (2004).
- [47] R. M. Lorenz, J. S. Edgar, G. D. Jeffries, Y. Zhao, D. McGloin, and D. T. Chiu, Vortex-trap-induced fusion of femtoliter-volume aqueous droplets, Anal. Chem. **79**, 224 (2007).
- [48] S. Fürhapter, A. Jesacher, S. Bernet, and M. Ritsch-Marte, Spiral phase contrast imaging in microscopy, Opt. Express 13, 689 (2005).
- [49] S. Fürhapter, A. Jesacher, S. Bernet, and M. Ritsch-Marte, Spiral interferometry, Opt. Lett. **30**, 1953 (2005).
- [50] C. Maurer, A. Jesacher, S. Bernet, and M. Ritsch-Marte, What spatial light modulators can do for optical microscopy, Laser Photon. Rev. 5, 81 (2011).
- [51] A. Mair, A. Vaziri, G. Weihs, and A. Zeilinger, Entanglement of the orbital angular momentum states of photons, Nature (London) **412**, 313 (2001).
- [52] M. Malik, M. Erhard, M. Huber, M. Krenn, R. Fickler, and A. Zeilinger, Multi-photon entanglement in high dimensions, Nature Photon. 10, 248 (2016).
- [53] K. Dholakia, N. B. Simpson, M. J. Padgett, and L. Allen, Second-harmonic generation and the orbital angular momentum of light, Phys. Rev. A 54, R3742 (1996).
- [54] J. T. Mendonça, B. Thidé, and H. Then, Stimulated Raman and Brillouin Backscattering of Collimated Beams Carrying

- Orbital Angular Momentum, Phys. Rev. Lett. **102**, 185005 (2009).
- [55] S. Ali, J. R. Davies, and J. T. Mendonca, Inverse Faraday Effect with Linearly Polarized Laser Pulses, Phys. Rev. Lett. 105, 035001 (2010).
- [56] G. Gariepy, J. Leach, K. T. Kim, T. J. Hammond, E. Frumker, R. W. Boyd, and P. B. Corkum, Creating High-Harmonic Beams with Controlled Orbital Angular Momentum, Phys. Rev. Lett. 113, 153901 (2014).
- [57] J. Vieira and J. T. Mendonça, Nonlinear Laser Driven Donut Wakefields for Positron and Electron Acceleration, Phys. Rev. Lett. 112, 215001 (2014).
- [58] J. Vieira, R. M. Trines, E. P. Alves, R. Fonseca, J. Mendonça, R. Bingham, P. Norreys, and L. Silva, Amplification and generation of ultra-intense twisted laser pulses via stimulated raman scattering, Nature Commun. 7, 10371 (2016).
- [59] Y. Shi, J. Vieira, R. M. G. M. Trines, R. Bingham, B. F. Shen, R. J. Kingham *et al.*, Magnetic Field Generation in Plasma Waves Driven by Copropagating Intense Twisted Lasers, Phys. Rev. Lett. 121, 145002 (2018).
- [60] R. Nuter, P. Korneev, and V. Tikhonchuk, Raman scattering of a laser beam carrying an orbital angular momentum, Phys. Plasmas **29**, 062101 (2022).
- [61] W. J. Tomlinson, Wavelength multiplexing in multimode optical fibers, Appl. Opt. 16, 2180 (1977).
- [62] J. R. Leger, External methods of phase locking and coherent beam addition of diode lasers, in *Surface Emitting Semiconduc*tor Lasers and Arrays, edited by G. A. Evans and J. M. Hammer (Academic Press, New York, 1993), Chap. 8.
- [63] T. Fan, Laser beam combining for high-power, high-radiance sources, IEEE J. Sel. Top. Quantum Electron. 11, 567 (2005).
- [64] A. Brignon, Coherent Laser Beam Combining (John Wiley & Sons, New York, 2013).
- [65] S. Zhou, F. W. Wise, and D. G. Ouzounov, Divided-pulse amplification of ultrashort pulses, Opt. Lett. **32**, 871 (2007).
- [66] E. Seise, A. Klenke, J. Limpert, and A. Tünnermann, Coherent addition of fiber-amplified ultrashort laser pulses, Opt. Express 18, 27827 (2010).
- [67] E. Seise, A. Klenke, S. Breitkopf, M. Plötner, J. Limpert, and A. Tünnermann, Coherently combined fiber laser system delivering 120 µi femtosecond pulses, Opt. Lett. **36**, 439 (2011).
- [68] L. Daniault, M. Hanna, L. Lombard, Y. Zaouter, E. Mottay, D. Goular, P. Bourdon, F. Druon, and P. Georges, Coherent beam combining of two femtosecond fiber chirped-pulse amplifiers, Opt. Lett. 36, 621 (2011).
- [69] A. Klenke, E. Seise, J. Limpert, and A. Tünnermann, Basic considerations on coherent combining of ultrashort laser pulses, Opt. Express 19, 25379 (2011).
- [70] M. Kienel, A. Klenke, T. Eidam, M. Baumgartl, C. Jauregui, J. Limpert, and A. Tünnermann, Analysis of passively combined divided-pulse amplification as an energy-scaling concept, Opt. Express 21, 29031 (2013).
- [71] A. Klenke, S. Hädrich, T. Eidam, J. Rothhardt, M. Kienel, S. Demmler, T. Gottschall, J. Limpert, and A. Tünnermann, Gw peak-power fiber chirped-pulse-amplification system, Opt. Lett. 39, 6875 (2014).
- [72] T. Zhou, J. Ruppe, C. Zhu, I.-N. Hu, J. Nees, and A. Galvanauskas, Coherent pulse stacking amplification using low-finesse gires-tournois interferometers, Opt. Express 23, 7442 (2015).

- [73] I. Fsaifes, L. Daniault, S. Bellanger, M. Veinhard, J. Bourderionnet, C. Larat, E. Lallier, E. Durand, A. Brignon, and J.-C. Chanteloup, Coherent beam combining of 61 femtosecond fiber amplifiers, Opt. Express 28, 20152 (2020).
- [74] D. Wang, Q. Du, T. Zhou, D. Li, and R. Wilcox, Stabilization of the 81-channel coherent beam combination using machine learning, Opt. Express **29**, 5694 (2021).
- [75] K. Y. Kim, J. H. Glownia, A. J. Taylor, and G. Rodriguez, Terahertz emission from ultrafast ionizing air in symmetry-broken laser fields, Opt. Express 15, 4577 (2007).
- [76] M. R. Edwards, V. T. Platonenko, and J. M. Mikhailova, Enhanced attosecond bursts of relativistic high-order harmonics driven by two-color fields, Opt. Lett. 39, 6823 (2014).

- [77] Q. Zhan, Cylindrical vector beams: From mathematical concepts to applications, Adv. Opt. Photon. 1, 1 (2009).
- [78] X.-L. Wang, Y. Li, J. Chen, C.-S. Guo, J. Ding, and H.-T. Wang, A new type of vector fields with hybrid states of polarization, Opt. Express 18, 10786 (2010).
- [79] G. Milione, H. I. Sztul, D. A. Nolan, and R. R. Alfano, Higher-Order Poincaré Sphere, Stokes Parameters, and the Angular Momentum of Light, Phys. Rev. Lett. 107, 053601 (2011).
- [80] D. Naidoo, F. S. Roux, A. Dudley, I. Litvin, B. Piccirillo, L. Marrucci, and A. Forbes, Controlled generation of higher-order poincaré sphere beams from a laser, Nat. Photon. 10, 327 (2016).
- [81] L. Debnath and F. A. Shah, Wavelet Transforms and Their Applications (Birkhäuser, Boston, 2015).